Oxidation of silicon nitride under standard air or microwave-excited air at high temperature and low pressure

M. BALAT, M. CZERNIAK, R. BERJOAN
Institut de science et de génie des Matériaux et Procédés (IMP-CNRS), BP5, 66125 Font-Romeu - Odeillo Cédex, France

During the atmospheric re-entry of space shuttles, the thermal constraints due to the hypersonic velocity can lead to very extensive damage on materials of the protective heat shield (oxidation, thermal shock, etc.). In order to test the oxidation resistance of such materials, we have realized an experimental set-up called MESOX which associates a concentrated radiation solar furnace and a microwave generator. The maximal heat flux is 4.5 MW m^{-2}, and the temperature ranges up to 2500 K. The total pressure is in the range 10^2–10^4 Pa. For silicon-based ceramics, it is necessary to have a good knowledge of the conditions for the existence of a protective silica layer. The determination of the transition between passive and active oxidation is done, in the case of sintered silicon nitride, under standard and microwave-excited air.

1. Introduction

Silicon-based ceramic materials which have a good oxidation resistance at high temperature are candidates for the thermal protection system (TPS) of the space plane structure which receives very high thermal fluxes (between 0.5 and 1 MW m^{-2}) during the atmospheric re-entry phase. Two main regimes govern the oxidation of these materials: the passive oxidation, with the formation of a protective silica layer leading generally to a mass gain of the sample, and the active oxidation, with vaporization of silicon monoxide leading to a mass loss of the sample and its degradation.

Many authors have worked on the silicon nitride oxidation, often in the passive domain, and some have established the possible existence of an intermediate oxynitride layer between Si_3N_4 and SiO_2 [1–5]. The oxidation kinetics has been amply studied, but the transition between passive and active oxidation is not well known. The determination of this transition is important to evaluate the domain where the silicon nitride is not damaged.

After a literature review, comparing the different theoretical and experimental results, theoretical thermodynamic calculations are performed, based on Eriksson and Wagner's models. Experimental tests were carried out on sintered silicon nitride under standard and dissociated air using a testing bench called MESOX (Moyen d'Essai Solaire d'OXydation) which associates a solar concentrator and a microwave generator.

2. Literature review

Table I gives the theoretical and/or experimental working conditions for the study of silicon nitride oxidation reported by several authors. Many authors [6–18] have worked on the silicon nitride oxidation but often in the passive domain. Only Singhal [6, 7], Vaughn and Maahs [13], Sheehan [11], Kim and Moorhead [14] and Narushima *et al.* [17] have studied the transition between active and passive oxidation, active oxidation occurring at low oxygen potentials. Fig. 1 shows the theoretical transition curves in terms of oxygen partial pressure versus inverse temperature for these author's results. The main differences between the results come from:

(i) the chemical nature of the Si_3N_4 material (chemical vapour deposited, sintered, hot-pressed with several per cent additive, reaction-bonded, etc);

(ii) the nature of the reacting gas (pure O_2, O_2–Ar, O_2–N_2, air, etc.);

(iii) the total pressure used (atmospheric or reduced);

(iv) and for the theoretical model, the calculation of the diffusion coefficient or the values taken for the thermodynamic data (ΔG_f°).

For example, in some cases, the total working pressure is near 10^5 Pa, so the oxidation proceeds in the viscous gas flow regime [6, 8–12, 14, 15, 17]. This situation is very different from working at low total pressure, and thus low oxygen partial pressure [9, 13, 18], in a molecular flow regime. This has recently been described for silicon carbide oxidation [19].

3. Theoretical thermodynamic study

Wagner's model [20], developed for silicon, was modified by Balat [19, 21–23] for SiC. It is well suited because it takes into account the mass transfer

0022–2461 © *1997 Chapman & Hall*

TABLE I Literature data, tests conditions and materials used for the oxidation of silicon nitride

Authors [ref.]	Si_3N_4 material	Gas	Flow ($cm^3 s^{-1}$)	P_{O_2} (Pa)	P total (Pa)	Method	Temperature range (K)
Singhal [7]	–	O_2	–	–	–	theory	–
Singhal [6]	β HPSN 1% MgO	Dry O_2 O_2–Ar N_2–O_2–Ar	8.33 to 83.33	10^3–9×10^4	10^5	TGA	1273–1673
Tripp [8]	HPSN	O_2, O_2–N_2, O_2–Ar, CO–CO_2	1.25	800–8×10^4	8×10^4–10^5	TGA	1573–1773
Warburton [9]	RBSN	air vacuum	1.66	2×10^4 –	10^5 3×10^{-3}– 3×10^{-2}	TGA	973–1373 1323–1473
Hirai [10]	CVD α	Dry O_2	8.33	10^5	10^5	TGA	1823–1923
Sheehan [11]	HPSN 1–5% MgO	O_2–He	8.33	0.4–0.8	1.5×10^5	furnace	1373–1473
Du [12]	CVD α	Dry O_2, O_2–Ar, O_2–N_2–Ar	5	5.06×10^3–10^5 5.06×10^4	10^5	–	1373–1673
Vaughn [13]	HPSN (MgO) sintered 6% Y_2O_3	Dry air	0.56	7–206	35–1030	TGA	1623–1793
Kim [14]	HPSN with 6% Y_2O_3, Al_2O_3 CVD	O_2–Ar	28.5	10^{-1}–10^3	10^5	furnace	1673
Ishikawa [15]	sintered 5% Y_2O_3, 5% Al_2O_3	O_2–N_2 O_2	0.33 to 1	10^2–10^5	10^5	furnace	1673
Narushima [16]	CVD α	Dry O_2	3.33	10^5	10^5	TGA	1923–2003
Narushima [17]	CVD α	O_2–N_2 O_2–Ar	1.53 to 49	0.5–120	10^5	TGA	1823–1923
Jimenez [18]	CVD α	O_2		2.5×10^3	2.5×10^3	RF plasma	473–1223

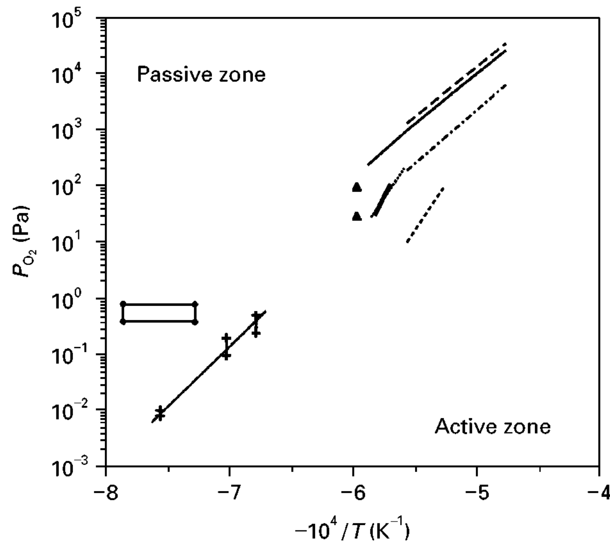

Figure 1 Theoretical transition curves giving oxygen partial pressure versus inverse temperature from: (——) present work for SiO_2 formation; (–·–·–) present work for Si_2N_2O formation; (– – –) Singhal [7]; (——) and (···) Vaughn and Maahs [13]; (– – –) Narushima *et al.* [17], (▲) Kim and Moorhead [14], (-●-) Sheehan [11] and (–‡–) Warburton *et al.* [9].

constraints (open system) and leads to the determination of the transition point in terms of oxygen partial pressure in the bulk gas. It has been used for silicon nitride oxidation.

First, Eriksson's model [24] is used to determine the major gaseous species present at the solid–gas interface. The equilibrium calculations are based upon the free-energy minimization method for constant temperature and pressure values. The constraints of the model are: a closed system, mass conservation and Duhem's phase rule.

Before passivation by the silica layer, the solid–gas interface is composed of the solid silicon nitride layer and the following gaseous species: SiO, O_2 and N_2.

During passive oxidation, a protective silica layer is formed through reaction

$$Si_3N_4(s) + 3O_2(g) = 3SiO_2(s) + 2N_2(g) \quad (1)$$

During active oxidation, silicon monoxide and nitrogen are vaporized via the reaction

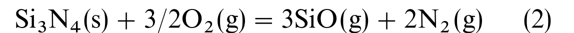

$$Si_3N_4(s) + 3/2O_2(g) = 3SiO(g) + 2N_2(g) \quad (2)$$

For each phase, the mass balance for each atomic compound is established and the interface mass conservation is applied.

The flux density, J_i, of the compound i at the interface, is expressed by Fick's law

$$J_i = -D_i(P_i^{\infty} - P_i^{w})/\delta_i RT \quad (3)$$

with D_i the mass transfer coefficient in the carrying gas (air), δ_i the thickness of the boundary concentration layer, R the perfect gas constant, T the temperature, P_i^{∞} the partial pressure of the species i in the bulk gas, and P_i^{w} the partial pressure of i at the interface.

In the gaseous phase

$$(J_O^G) = 2J_{O_2}^G + J_{SiO}^G \quad (4a)$$

$$(J_{Si}^G) = J_{SiO}^G \quad (4b)$$

$$(J_N^G) = 2J_{N_2}^G \quad (4c)$$

In the condensed phase

$$(J_{O}^{S}) = 0 \quad (5a)$$

$$(J_{Si}^{S}) = 3J_{Si_3N_4}^{S} \quad (5b)$$

$$(J_{N}^{S}) = 4J_{Si_3N_4}^{S} \quad (5c)$$

Accounting for the principle of mass conservation at the interface, the following system is obtained

$$2J_{O_2}^{G} + J_{SiO}^{G} = 0 \quad (6a)$$

and

$$3J_{N_2}^{G} = 2J_{SiO}^{G} \quad (6b)$$

with the two hypotheses $P_{O_2}^{w} = 0$ (interface consumption) and $P_{SiO}^{\infty} = 0$ (boundary concentration layer), and with the approximation of Wagner (laminar flow)

$$(D_{SiO}/D_{O_2})^{1/2} = \delta_{SiO}/\delta_{O_2} \quad (7)$$

Equation 6 is reduced to

$$P_{O_2}^{\infty} = (1/2)(D_{SiO}/D_{O_2})^{1/2} P_{SiO}^{w} \quad (8a)$$

and

$$P_{N_2}^{w} = P_{O_2}^{\infty}[4 + (4/3)(D_{N_2}/D_{O_2})^{-1/2}] \quad (8b)$$

Then, the oxygen partial pressure is expressed in terms of thermodynamical parameters accounting with Equations 1 and 2, with the two equilibrium constants K_1 and K_2

$$P_{O_2}^{\infty} = 0.595(D_{SiO}/D_{O_2})^{3/8} \times [4 + (4/3)(D_{N_2}/D_{O_2})^{-1/2}]^{-1/4} K_1^{-1/8} K_2^{1/4} \quad (9)$$

Calculating the diffusion coefficients by the Chapman–Enskog theory [25], Equation 9 becomes (at 2000 K)

$$P_{O_2}^{\infty} = 0.288 K_1^{-1/8} K_2^{1/4} \quad (10)$$

Table II gives the values of the temperatures and the partial pressures of oxygen in the bulk gas for the transition zone of this work. The calculations are based on the thermodynamic data of the Thermodata bank [26], Janaf tables [27], Paneck [28] and Hillert *et al.* [29]. The differences between the theoretical results arise from the ΔG_f° (Si_3N_4) values: for example, at 1900 K, for Paneck, the value is -131.97 kJ mol^{-1}, from Thermodata, it is only -50.43 kJ mol^{-1} and for Hillert *et al.* the value is an intermediate one of -81 kJ mol^{-1}.

Fig. 1 shows the transition lines between active and passive oxidation for this work (theoretical result) and for literature data (experimental results). Similar thermodynamical calculations under dissociated air show no difference in the transition zone position with the calculations under standard air.

A study taking into account the formation of an intermediate oxynitride layer, Si_2N_2O, has also been realized and shows a movement in the active zone. In Table II, the theoretical results are given for various authors. As in the previous case, the differences arise from the $\Delta G_f^\circ(Si_3N_4)$ and $\Delta G_f^\circ(Si_2N_2O)$ values: for example, at 1900 K, the values for $\Delta G_f^\circ(Si_2N_2O)$ are -406.18 kJ mol^{-1} for Fegley [30], -455.00 kJ mol^{-1} for Hillert *et al.* [29] and -343.25 kJ mol^{-1} from the Thermodata bank [26].

Our theoretical results are compared with those of Singhal [6]; the difference can be attributed to the values of the diffusion coefficients and the choice of the thermodynamic data. The experimental results of Vaughn and Maahs [13] for hot-pressed and sintered silicon nitride, of Kim and Moorhead [14] for HP and CVD materials, and of Sheehan [11], are not so different from ours. Those of Narushima *et al.* [17] for CVD Si_3N_4 are located at lower oxygen partial pressure, this could be due to the chemical nature of the Si_3N_4; this phenomenon was already observed on SiC [19].

For Warbuton *et al.*'s results [9], it is more a decomposition of the silicon nitride than an oxidation process, the total pressure being very low (vacuum conditions).

4. Experimental procedure

The experimental apparatus, called MESOX, is shown in Fig. 2. It is composed of a cylindrical quartz vessel (1) 500 mm high and 50 mm diameter, which crosses the wave guide (10). Inside the vessel, alumina tubes with a zirconia sample-holder (3) support the materials. The microwave generator (8) (0–1200 W, 2450 MHz) works at a constant power of 300 W for the presented results. The incident and reflected powers are measured (9).

TABLE II Theoretical values of the transition points ($P_{O_2}^{\infty}$, T) for the oxidation of silicon nitride for the data of the Thermodata bank, Janaf tables and other, with formation of oxynitride or silica

T (K)	$P_{O_2}^{\infty}$ (Pa) → SiO_2				$P_{O_2}^{\infty}$ (Pa) → Si_2N_2O		
	Janaf	Thermodata	[a]Panek + Thermodata	[b]Hillert + Thermodata	[c]Fegley + Janaf	[b]Hillert + Thermodata	Thermodata
1600	47	51		37	0.6	0.06	8
1700	217	242	119	188	4	0.4	43
1800	832	967	491	755	21	1.5	189
1900	2740	3315	1739	2603	96	6	707
2000	7967	9997	5405	7901	371	18	2298
2100	20817	26770		21307	1252	53	6649
2200	49611	65243		52332	3761		17391

a: $\Delta G_f^\circ(Si_3N_4)$ from Panek (1995), other values from Thermodata (1994).
b: $\Delta G_f^\circ(Si_3N_4)$ and/or $\Delta G_f^\circ(Si_2N_2O)$ from Hillert (1990), other values from Thermodata (1994).
c: $\Delta G_f^\circ(Si_2N_2O)$ from Fegley (1981), other values from Janaf (1985).

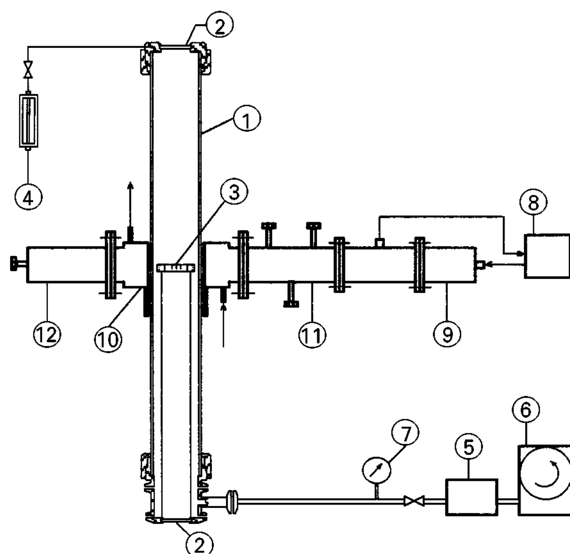

Figure 2 Experimental set-up MESOX: (1) quartz chamber, (2) viewports, (3) sample-holder, (4) flowmeter, (5) pressure regulator, (6) vacuum pump, (7) pressure gauge, (8) microwave generator, (9) isolator and power monitor, (10) refrigerated wave guide, (11) three-stubs tuner, (12) plunger.

This device is placed at the focus of a solar furnace, in which the heat fluxes can reach 4.5 $MW\,m^{-2}$; thus elevated temperatures on materials such as Si_3N_4 may be obtained. A regulator (5) and a gauge (7) are used to control precisely the pressure during the experiment. The pressure range is about 10^2–10^5 Pa for standard air and 10^2–5×10^3 Pa for dissociated air.

An optical pyrometer equipped with a filter centred at 5 μm gives the colour temperature of the front and back faces of the sample (measurement zone = 30 mm^2). Measurement is performed through CaF_2 viewports (2) and two fixed and one rotating mirrors. The correction of the temperature due to the emittance is done a posteriori with a value of 0.96 for the sintered silicon nitride at this wavelength [31].

5. Results

The samples were sintered β-Si_3N_4 (apparent bulk density 3.20×10^3 $kg\,m^{-3}$, theoretical density 3.28×10^3 $kg\,m^{-3}$) containing about 15% impurities (< 4% Al, 7% Y, 4% O) and were produced by "Céramiques et Composites" (France). The sample dimensions were 25 mm diameter and 3 mm high.

5.1. Experimental protocol

The pressure and the gas flow (1.11×10^{-6} $m^3\,s^{-1}$) conditions were fixed before each experiment. For the experiments under plasma, the microwave was switched on after pressure stabilization and before solar heating.

The temperature increase was controlled by the gradual opening of the shutter placed between the sample and the concentrated solar radiation, and was about 4 $K\,s^{-1}$. At the desired temperature, the level was maintained for 600 s and sample cooling was regulated at 2 $K\,s^{-1}$. The duration of the plateau was large enough to indicate the active oxidation regime. In fact, during the temperature increase and decrease at every pressure, silica formation takes place. However, on the temperature plateau, when active oxidation occurs, the surface of silicon carbide is very damaged and the silica formation with decreasing the temperature does not affect the phenomenon, as is revealed by scanning electron micrographs (SEM).

The modification of the sample is controlled by optical microscopy, weighing, X-ray diffraction, SEM and X-ray photoelectron spectroscopy (XPS).

5.2. Experiments under standard air

The results are presented in Fig. 3 and Table III. The samples A, B, C, D, R, F and K are covered with a thin silica layer (α-SiO_2) detected in some cases by X-ray diffraction. No intermediate layer of oxynitride Si_2N_2O, was detected by XPS. The weight gains were, respectively, 0.03%, 0.04%, 0.16%, 0.08%, 0.19%, 0.2% and 0.02%. All these samples were under passive oxidation.

For the samples E, J, G, P and M, the surface was damaged, and the weight losses were, respectively − 0.77%, − 1.2%, − 0.28%, − 0.05% and − 0.22%. The oxidation was active with vaporization of SiO and N_2.

For the samples L and N, α-SiO_2 was revealed by X-ray diffraction, with bubbles on the surface and a weak weight loss. The oxidation was near to the transition, but was passive.

Fig. 4 shows scanning electron micrographs of the sample before oxidation (reference) at magnifications of 500 and 2000, and for the samples F (silica layer, smooth surface) and E (active oxidation, surface damaged). The experiments realized under standard air are not so different from the theoretical calculations. The weak difference can be attributed to the sintering aids which modify the oxidation kinetics [11].

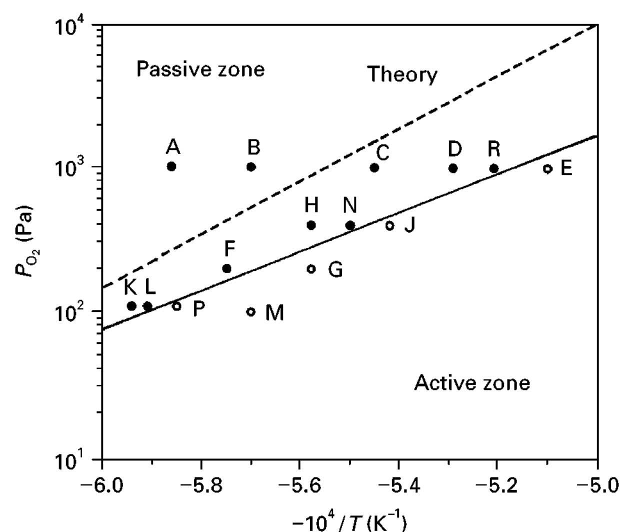

Figure 3 Position of the transition zone between active and passive oxidation under standard air. (●) Samples A, B, C, D, R, F, H, N, L and K with a passive silica layer; (○) samples E, J, G, P and M under active oxidation.

TABLE III Experimentals points under standard air (a/p is for active/passive)

Sample	A	B	C	D	E	F	G	H	J	K	L	M	N	P	R
T (K)	1705	1755	1834	1892	1960	1734	1793	1793	1846	1686	1695	1752	1817	1710	1920
$P^{\infty}_{O_2}$ (Pa)	1000	1000	1000	1000	1000	200	200	400	400	120	100	100	400	120	1000
a/p	p	p	p	p	a	p	a	p	a	p	p	a	p	a	p

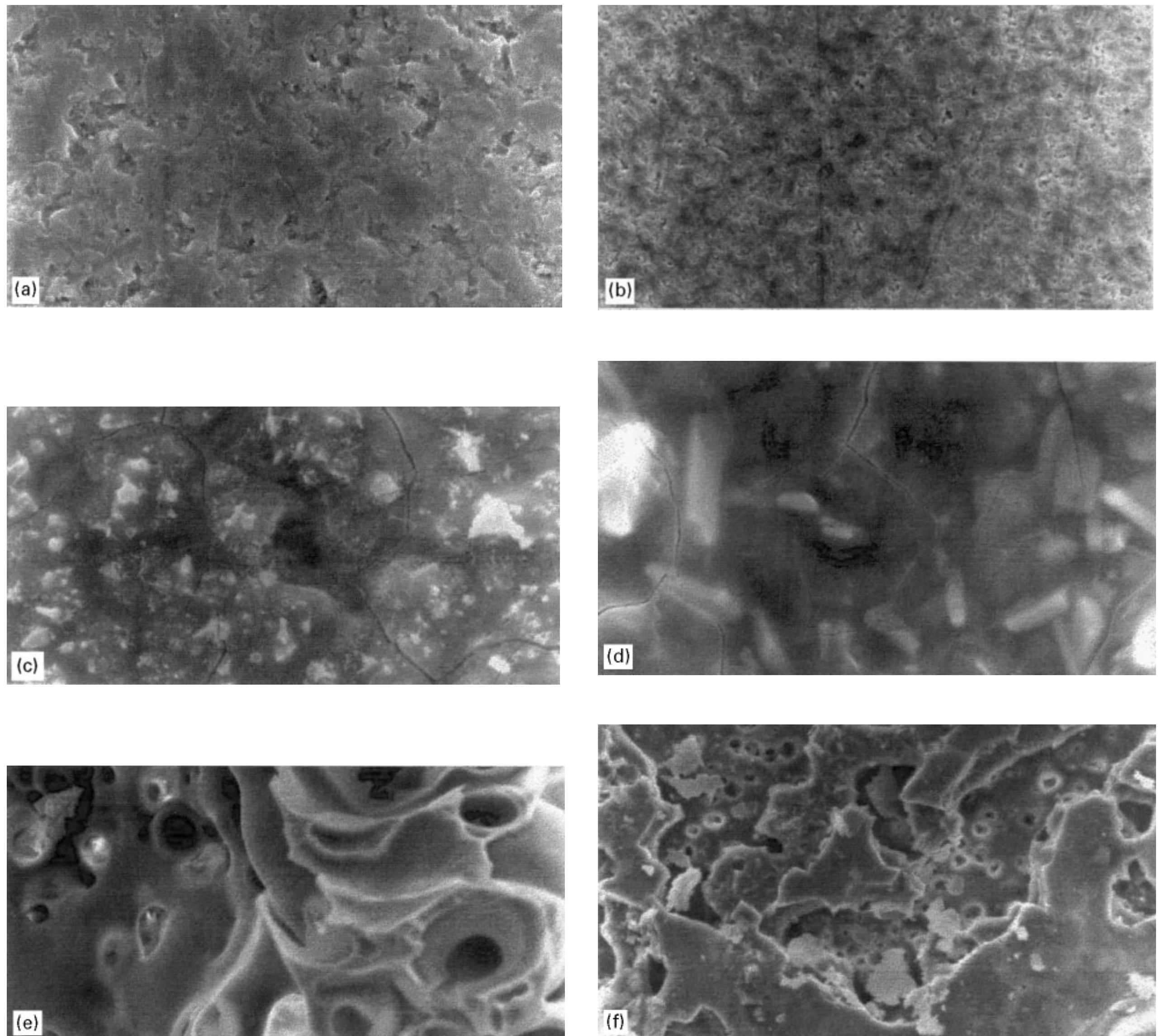

Figure 4 Scanning electron micrographs of silicon nitride samples: (a, b) reference, before oxidation, (a) ×2000 and (b) ×500, (c) F and (d) Q′ after passive oxidation (×2000), (e) E and (f) T′ after active oxidation (×500).

5.3. Experiments under microwave-excited air

The results under dissociated air are represented in Fig. 5 and given in Table IV. Samples S′, K′, B′, A′ and V′ present a thin silica layer on the surface leading to a weight gain, respectively, of 0.2%, 0.2%, 0.1%, 0.09% and 0.02%, whereas samples L′, C′, X′, T′ and W′ have weight losses of −5%, −1.4%, −0.8%, −0.9% and −0.04%, respectively. The sample Q′ has bubbles on the surface and no weight change; the oxidation was near the transition, but in the passive domain.

On the contrary to the case of SiC [19], the transition line under microwave-excited air is located at nearly the same pressure for the temperature range.

Fig. 4 shows scanning electron micrographs for the samples Q′ (silica layer, smooth surface) and T′ (active oxidation, surface damaged).

Figs 6 and 7 show the XPS valence band spectra and the Si *KLL* Auger transitions collected for samples labelled X, C′, Q′ and K′. X is the untreated sample of the Si_3N_4 material used in this work. Note that the material contains about 4% weight oxygen, as given by the manufacturer. Sample C′ was a sample heated at 1915 K under “active oxidation” conditions. Samples Q′ and K′ were heated under “passive oxidation” conditions.

The XPS valence band and Auger Si *KLL* spectra were collected after a slight mechanical polishing of the surfaces. This polishing was identical for all the

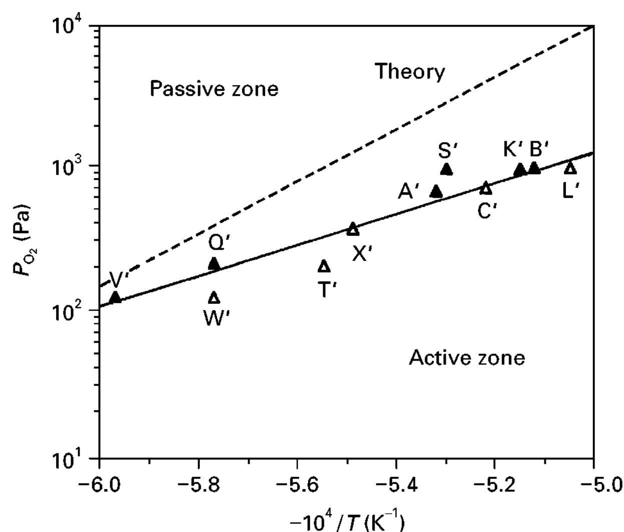

Figure 5 Position of the transition zone between active and passive oxidation under microwave-excited air. (▲) Samples S′, K′, B′, A′, Q′ and V′ with a passive silica layer, (△) samples L′, C′, X′, T′ and W′ under active oxidation.

samples. Then, in the ultra-high vacuum chamber, the surfaces were sputtered by an argon-ion beam accelerated under 4 kV. These samples are insulating materials. Therefore, the ionic bombardment was probably not very effective. Moreover, large charging effects, leading to shifts of the characteristic electron peaks were observed. So the energy position of the peaks was normalized with the O_{2s} peak, assuming that the binding energy of the O_{2s} electronic level does not change significantly with changing sample composition [5, 32].

The valence band spectrum collected on sample X (as-received Si_3N_4 sample), shown in Fig. 6, is similar to the spectrum reported elsewhere [32, 33]. This spectrum is constituted by three electronic band levels having N_{2p_z} character, in the energy range 3–4 eV, Si_{3p}–$N_{2p_{xy}}$ mixed character near 7 eV and Si_{3s}–$N_{2p_{xy}}$ mixed character near 11 eV.

The valence band spectrum collected for sample K′ is similar to the spectrum reported for silica [34]. The three main peaks present in this last valence band spectrum result from the emission of O_{2p_z} electrons having a binding energy near 8 eV, and from the emission of valence band levels having mixed characters Si_{3p}–$O_{2p_{xy}}$ near a binding energy of 11 eV, or Si_{3s}–$O_{2p_{xy}}$ near 14 eV.

For sample C′, the three main features observed for sample X are also detected. However, slight shifts of the photoelectron peaks are observed when comparing the valence band spectrum of C′ with that of X. Moreover, a fourth peak, having a low intensity, is observed in the C′ spectrum. The differences between

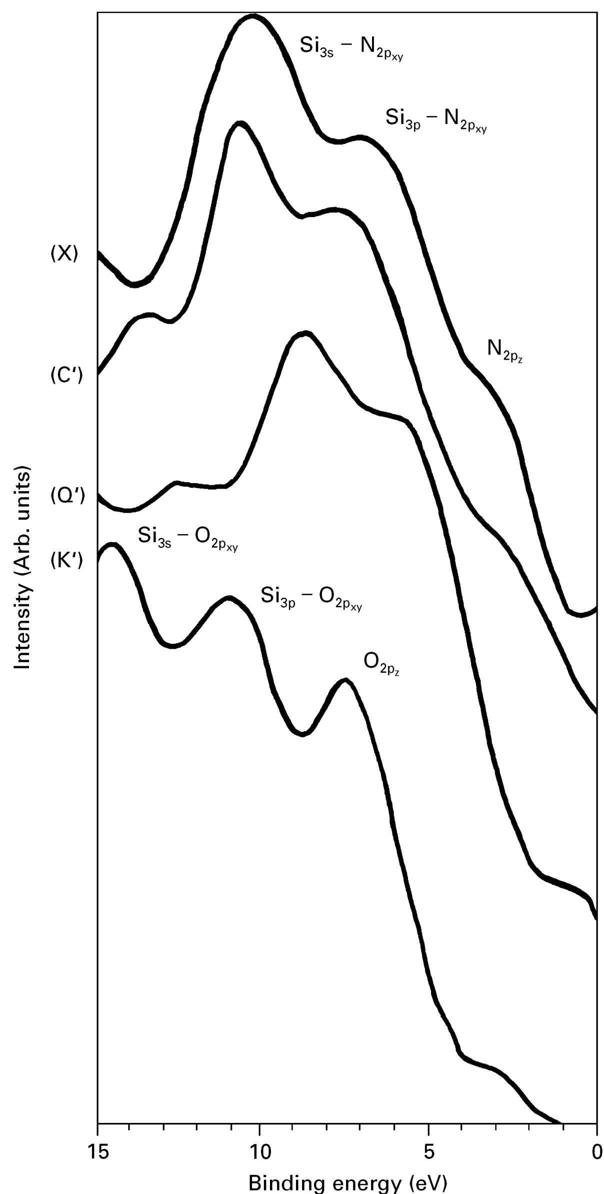

Figure 6 XPS valence band spectra for the samples X (reference material Si_3N_4), C′ (under active oxidation), Q′ and K′ (under passive oxidation).

the C′ and X (reference sample) spectra may be attributed to the presence of a higher contribution of Si–O bonds for C′ than for X.

The Q′ spectrum is very different from the X spectrum – essentially Si–N bonds – and from the K′ spectrum – essentially Si–O bonds. This spectrum results probably from a mixing of Si_3N_4 and SiO_2 chemical bonds [35].

The Si *KLL* Auger transitions presented in Fig. 7 confirm the information provided by the valence band spectra study. All the Si *KLL* spectra present two features. The first one, located near 1612.5 eV, is

TABLE IV Experimentals points under microwave-excited air (a/p is for active/passive)

Sample	A′	B′	C′	K′	L′	Q′	S′	T′	V′	W′	X′
T (K)	1878	1952	1915	1940	1980	1730	1885	1802	1670	1730	1822
$P^{\infty}_{O_2}$ (Pa)	700	1040	730	1000	1030	220	1000	200	120	120	380
a/p	p	p	a	p	a	p	p	a	p	a	a

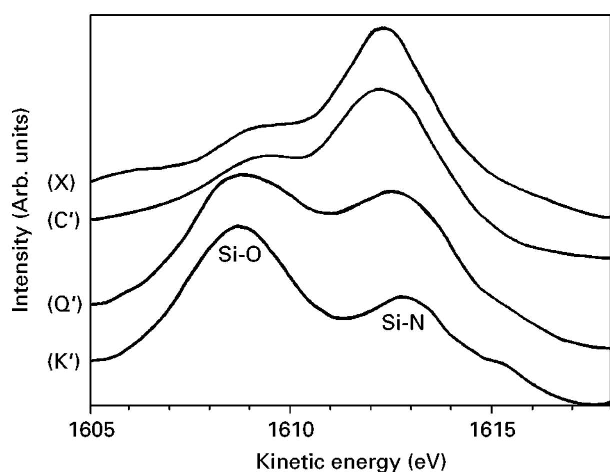

Figure 7 Si *KLL* Auger transitions for the samples X (reference material Si_3N_4), C′ (under active oxidation), Q′ and K′ (under passive oxidation).

currently attributed to Si–N bonds in Si_3N_4 compounds [36]. The second one, located between 1608.5 and 1609.5 eV, is due to the Si *KLL* electrons emitted from silica [37, 38]. The change of the Si *KLL* kinetic energy between 1608.5 eV for samples X and C′ containing a major contribution of Si–N bonds, and 1609.5 eV for samples Q′ and K′ having a major contribution of Si–O bonds, may be due to the presence of SiO_x ($x < 2$) substoichiometric silicon oxides in the sample X and C′ [38].

None of the Si *KLL* spectra indicates the presence of high-temperature crystallized Si_2N_2O compound [35]. All of them are characteristic of SiO_2 (or SiO_x) and Si_3N_4 mixtures.

The Si *KLL* spectrum of the C′ sample confirms that this sample was treated under "active oxidation" conditions, as revealed by the low Si–O bonds contribution. On the contrary, the Si *KLL* spectra for samples Q′ and K′ show the predominance of the peak near 1608.5 eV, resulting from the presence of a large silica content. This result is in good agreement with the "passive oxidation" conditions.

6. Conclusion

The experimental study of the oxidation of sintered silicon nitride at high temperature and low pressure allows establishment of the transition zone between active and passive oxidation under standard and microwave-excited air.

The comparison of theoretical calculations and experimental results shows a small difference which can be attributed to the sintering aids or to the used theoretical model which takes into account a diffusional control for the oxidation reaction, but the reaction may be under chemical control or a mixed one.

The influence of the sintering aids can be evaluated using Si_3N_4 obtained by chemical vapour deposition (CVD).

From the X-ray diffraction spectra and the experimental transition line, it seems that no oxynitride intermediate layer is formed; this is confirmed by XPS spectroscopy.

Oxidation experiments, under dissociated air, had never before been realized on Si_3N_4, and the results show almost no difference with those under molecular air.

References

1. L. U. T. OGBUJI, *J. Am. Ceram. Soc.* **75** (1992) 2995.
2. L. U. T. OGBUJI and S. R. BRYAN, *ibid.* **78** (1995) 1272.
3. L. U. T. OGBUJI, *ibid.* **78** (1995) 1279.
4. K. E. SPEAR, R. E. TRESSLER, Z. ZHENG and H. DU, *Ceram. Trans.* **10** (1990) 1.
5. H. DU, Thesis in Ceramic Sciences, The Pennsylania State University, USA (1988).
6. S. C. SINGHAL, *J. Mater. Sci.* **11** (1976) 500.
7. *Idem, Ceram. Int.* **2** (1976) 123.
8. W. C. TRIPP and H. C. GRAHAM, *J. Am. Ceram. Soc.* **59** (1976) 399.
9. J. B. WARBURTON, J. E. ANTILL and R. W. M. HAWES, *ibid.* **61** (1978) 67.
10. T. HIRAI, K. NIHARA and T. GOTO, *ibid.* **63** (1980) 419.
11. J. E. SHEEHAN, *ibid.* **65** (1982) C111.
12. H. DU, R. E. TRESSLER, K. E. SPEAR and C. G. PANTANO, *J. Electrochem. Soc.* **136** (1989) 1527.
13. W. L. VAUGHN and H. G. MAAHS, *J. Am. Ceram. Soc.* **73** (1990) 1540.
14. H. E. KIM and A. J. MOORHEAD, *ibid.* **73** (1990) 3007.
15. M. ISHIKAWA, N. TAKEUCHI, S. ISHIDA, M. WAKAMATSU and K. WATANABE, *J. Ceram. Soc. Jpn* **99** (1991) 1084.
16. T. NARUSHIMA, R. Y. LIN, Y. IGUCHI and T. HIRAI, *J. Am. Ceram. Soc.* **76** (1993) 1047.
17. T. NARUSHIMA, T. GOTO, Y. YOKOYAMA, J. HAGIWARA, Y. IGUCHI and T. HIRAI, *ibid.* **77** (1994) 2369.
18. C. JIMENEZ, J. PERRIERE, I. VICKRIDGE, J. P. ENARD and J. M. ALBELLA, *Surf. Coatings Technol.* **45** (1991) 147.
19. M. BALAT, *J. Eur. Ceram. Soc.* **16** (1996) 55.
20. C. WAGNER, *J. Appl. Phys.* **29** (1958) 1295.
21. M. BALAT, G. FLAMANT, G. MALE and G. PICHELIN, *J. Mater. Sci.* **27** (1992) 697.
22. M. BALAT, P. PEZE, M. LEBRUN and G. OLALDE, *Surf Coatings Technol.* **60** (1993) 587.
23. M. BALAT, C. DUPUY and D. MOCAER, *J. High Temp. Chem. Processes* **4** (1995) 25.
24. G. ERIKSSON, *Chem. Scripta* **8** (1973) 100.
25. R. D. BIRD, W. E. STEWARD and E. N. LIGHTFOOT, "Transport phenomena" (Wiley, New York, 1960).
26. THERMODATA, Université de Grenoble, 38402 St Martin d'Hères, France.
27. M. W. CHASE, J. R. DAVIES, J. R. DOWNEY, D. J. FRURIP, R. A. McDONALD and A. N. SYUERUD, "JANAF Thermodynamical Tables", 3rd Edn *J. Phys. Ref. Data* **14** (1985).
28. Z. PANEK, *J. Am. Ceram. Soc.* **78** (1995) 1087.
29. M. HILLERT, S. JONSSON and B. SUNDMAN, *Z. Metallkde* **83** (1992) 648.
30. B. Jr. FEGLEY, *J. Am. Ceram. Soc.* **64** (1981) C-124.
31. Y. S. TOULOUKIAN and D. P. De WITT, "Thermal radiative properties – Nonmetallic solids", Vol. 8 (Plenum, New York, 1972).
32. L. ORTEGA, Thèse de Doctorat, Universitè de Grenoble I, France (1993).
33. F. BOSCO and P. AVOURIS, *Phys. Rev. B* **38** (1988) 3937.
34. F. G. BELL and L. LEY, *Phys. Chem. B* **37** (1988) 8383.
35. R. SAOUDI, G. HOLLINGER and A. STRABONI, *J. Phys. III Fr.* **4** (1994) 881.
36. J. A. TAYLOR, *Appl. Surf. Sci.* **7** (1981) 168.
37. C. D. WAGNER, D. E. PASSOJA, H. F. HILLERY, T. G. KINISKY, H. A. SIX, W. T. JANSEN and J. A. TAYLOR, *J. Vac. Sci. Technol.* **21** (1982) 933.
38. R. BERJOAN, E. BECHE, J. A. ROGER and C. H. S. DUPUY, *J. High Temp. Chem. Process.* **3** (1994) 555.

Received 16 February
and accepted 31 July 1996